Physica D 454 (2023) 133867

Contents lists available at ScienceDirect

Physica D

journal homepage: www.elsevier.com/locate/physd

Bulges at vortical outflows

E.R. Johnson

Department of Mathematics, University College London, Gower Street, London WC1E 6BT, United Kingdom

ARTICLE INFO

Article history:
Received 30 November 2022
Received in revised form 13 July 2023
Accepted 25 July 2023
Available online 31 July 2023
Communicated by D. Pelinovsky

Keywords:
Rotating flow
Free boundary problem
Hodograph plane
Complex analysis
Coastal flow
Vorticity

ABSTRACT

This paper constructs steady solutions of the two-dimensional Euler equations corresponding to a line source of vortical fluid on the impermeable boundary of a quiescent flow. The nonlinear, free-boundary problem is solved by mapping the flow domain to the hodograph plane. A vortex dipole or, equivalently, a source–sink doublet is superposed on the source leading to flow patterns that model the ballooning outflows observed where rivers and straits discharge into the open ocean and in the rotating flow experiments and numerical simulations designed to reflect these observations.

1. Introduction

Observations by Lake et al. [1] and numerical modelling by Beardsley et al. [2], Spall and Price [3] and Marques et al. [4] show that fluid expelled from an outflow can gain positive or negative relative vorticity through the stretching and squashing of the expelled vortex columns. Motivated by these discussions, Johnson et al. [5] present a simple, fully nonlinear, dispersive, quasi-geostrophic model to describe the form of coastal outflows as the relative strength of vortex to Kelvin wave driving is varied and Jamshidi and Johnson [6] give a further discussion of finite-amplitude effects. When vertical density variations are sufficiently small the driving by image vorticity dominates Kelvin wave effects and the governing equations for constant depth flow reduce to the two-dimensional Euler equations, as demonstrated experimentally by Hide [7]. Johnson and McDonald [8], JM here, describe the coastal flow development in this limit for the initial value problem when a line source of vortical fluid against a wall is switched on, obtain an explicit analytical solution for the steady flow that is eventually set up and present numerical integrations, using the method of contour dynamics of the time-dependent two-dimensional Euler equations, that asymptote to the steady solution at large time.

One feature that is apparent in experiments modelling outflows [9] and numerical simulations of both the experiments [10] and observations [11,12], but not in the steady solutions of JM, is a bulging or ballooning of the vortical current in the neighbourhood of the outflow. Nof and Pichevin [13] argue that outflows are necessarily unsteady but Johnson et al. [5] and Southwick et al. [14] note that their momentum imbalance argument does not always apply and that the steady flow of JM expels downstream momentum from the source at precisely the rate that momentum is carried away in the far-field. The aim of the present paper is to extend the JM solutions to construct a steady ballooning outflow that is an exact solution of the two-dimensional Euler equations. When a vortex dipole or,equivalently, a source–sink doublet [15], injecting upstream momentum and so decreasing the net downstream momentum injected by the source, is superposed on the source then a ballooning steady recirculating region appears in the neighbourhood of the origin.

Section 2 gives the geometry, scalings and governing equations for the motion. Section 3 derives the steady solution for dipoles sufficiently strong for the flow to bulge near the outflow. Section 4 considers briefly the dynamics of perturbations to the steady solutions and Section 5 presents the numerical integration of an initial value problem that converges to the corresponding steady solution. The results are discussed briefly in Section 6 and Appendix A gives the solution for weak dipoles.

2. Governing equations

Consider the two-dimensional motion driven when inviscid fluid of uniform vorticity is expelled through a line source against a wall into initially quiescent irrotational fluid. The flow also gives the two-dimensional motion driven when irrotational inviscid fluid is expelled through a line source on a wall bounding fluid where the fluid and wall are in solid body rotation about an axis parallel to the axis of the line source: in the rotating frame

E-mail address: e.johnson@ucl.ac.uk.

https://doi.org/10.1016/j.physd.2023.133867

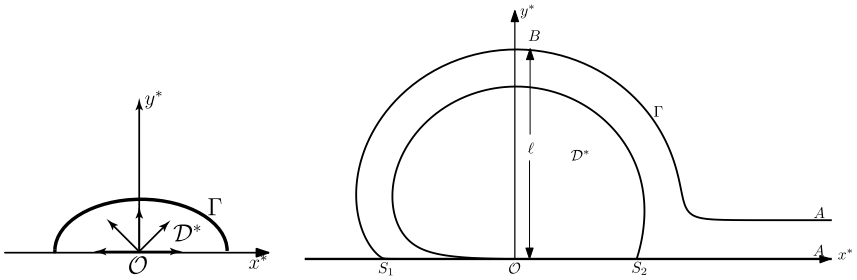

Fig. 1. (a) The vortical region at early time. (b) The scaling based on the final steady state.

the motion is that of a line source of fluid of constant vorticity on a stationary wall. There is no limitation on the speed of rotation or the strength of the outflow. Let there be superposed on the source flow a vortex dipole or, equivalently, a source–sink doublet directed so as to oppose the advection of vortical fluid by its image. This closely models the experimental setup in [9] where a source of constant-relative-vorticity fluid is located near the wall of a rapidly rotating tank, giving a clockwise or anticyclonic vortex which combines with its cyclonic image in the wall to give a vortex dipole at the outflow. As noted in JM, the same effect occurs if a source–sink pair on the tank wall is considered in the dipole limit where the source–sink separation goes to zero while the strengths go to infinity.

Take Cartesian axes Ox^*y^* with the impermeable wall lying along $y^* = 0$ and fluid expelled into the half-plane $y^* > 0$ from a source, at the origin O, with area flux Q (i.e. volume flux per unit distance perpendicular to the x^*y^* plane). Let the vorticity of the expelled fluid be ω and the strength of the dipole at the origin be $\mu*$, with dimensions of area flux times horizontal length. Since solutions for $\omega < 0$ follow by reflecting those for $\omega > 0$ about $x^* = 0$, ω can be taken as positive. The expelled fluid then propagates to the right under the influence of its image vorticity in the wall and so the vortex dipole is directed to the left with negative vorticity at $y^* = 0^+$ opposing the expelled vorticity. All expelled fluid eventually travels downstream in a unidirectional current of width $(2Q/\omega)^{1/2}$.

The formulae derived below take their simplest form by choosing the spatial scale for the flow to be the breadth of the vortical current at its widest point, denoted here by ℓ, and introducing the non-dimensional variables

$$(x^*, y^*) = \ell(x, y), \qquad (u^*, v^*) = \omega\ell(u, v), \qquad t = \omega t^*, \tag{1}$$

where (u^*, v^*) are the Cartesian velocity components and t^* time. For strong dipoles the flow balloons near the origin, $\ell > (2Q/\omega)^{1/2}$ and the downstream current has non-dimensional width $\alpha = (2Q/\omega\ell^2)^{1/2} < 1$. For weak dipoles the current is widest downstream and $\ell = (2Q/\omega)^{1/2}$ as for a simple source in JM. In both cases the strength of the dipole relative to that of the vorticity in the expelled fluid, $\mu = \mu^*/\omega\ell^3$, is the sole free parameter and is determined as part of the solution. For strong dipoles μ is obtained in Section 3 as a function of α and for weak dipoles in Appendix A as a function of c where $c\,\omega\ell$ is the maximum downstream velocity.

Incompressibility allows the introduction of a streamfunction ψ defined through $(u, v) = (-\psi_y, \psi_x)$. Then at each time t the flow consists of the vortical fluid occupying an expanding region $\mathcal{D}$ (say) bounded by the wall and an advancing front Γ separating vortical fluid from irrotational fluid (Fig. 1(a)). The streamfunction thus satisfies

$$\nabla^2\psi = \begin{cases} 1 & \text{in } \mathcal{D} \\ 0 & \text{outside } \mathcal{D} \end{cases} \tag{2a}$$

$$\psi = \begin{cases} 0 & y = 0, \quad x < 0 \\ Q/2\omega\ell^2 & y = 0, \quad x > 0 \end{cases} \tag{2b}$$

$$\psi \to 0 \qquad \text{as } x^2 + y^2 \to \infty \text{ (outside } \mathcal{D}), \tag{2c}$$

together with the superposition of an irrotational dipole at the origin, which identically satisfies the homogeneous form of (2). System (2), with the condition that ψ and $\nabla\psi$ are continuous across Γ, uniquely determines ψ at each instant. The evolution of the flow is given simply by the movement of the front Γ, with for each (x, y) on Γ,

$$\dot{x} = u(x, y, t), \qquad \dot{y} = v(x, y, t), \tag{3}$$

where the overdot denotes differentiation with respect to time, t. Section 5 presents numerical integrations of the initial value problem for the evolution of this system when the source and dipole are switched on in a previously quiescent fluid, comparing the asymptotic state with the corresponding steady solution derived below.

3. The exact steady state for strong dipoles

For most dipole strengths the greatest current width occurs across the ballooning region (Fig. 1(b)) and this will be the case presented here. The modification for weak dipoles, where the greatest width occurs downstream is noted in Appendix A. In steady flow the front Γ is a streamline meeting the wall at a stagnation point S_1 (say) in $x < 0$. Since the flow is smooth in the neighbourhood of Γ,

$$\psi = 0 \qquad \text{on } \Gamma. \tag{4}$$

Thus ψ is identically zero outside $\mathcal{D}$ and the flow outside $\mathcal{D}$ is stagnant. The steady solution is thus governed by (2) with (2c) replaced by

$$\nabla\psi = 0 \qquad \text{on } \Gamma. \tag{5}$$

Consider (following Howison and King [16])

$$w_0(z) = \bar{z} - 2(v + \mathrm{i}u) = v_0 + \mathrm{i}u_0, \tag{6}$$

($z = x + \mathrm{i}y$, $\bar{z} = x - \mathrm{i}y$). It follows directly from (2) that $w_0(z)$ is an analytic function of z in $\mathcal{D}$ with the exception of singularities at the origin: a simple pole giving the fluid source and a double pole giving the dipole. Moreover (5) shows that

$$w_0(z) = \bar{z} \qquad \text{on } \Gamma. \tag{7}$$

Thus $w_0(z) = S(z)$ (say), the Schwarz function for the curve Γ.

Equivalently, and perhaps more fundamentally, Crowdy [17] and Crowdy [18] (chap. 24) shows that the streamfunction can be identified as the modified Schwarz potential

$$\psi = -\frac{1}{4}\left(z\bar{z} - \int^z S(z')\,\mathrm{d}z' - \overline{\int^z S(z')\,\mathrm{d}z'}\right), \tag{8}$$

with associated velocity field

$$u - \mathrm{i}v = 2\mathrm{i}\frac{\partial\psi}{\partial z} = -\frac{\mathrm{i}}{2}[\bar{z} - S(z)]. \tag{9}$$

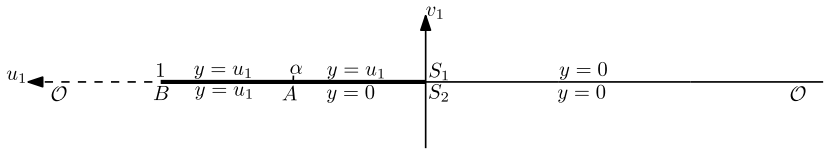

Fig. 2. The cut hodograph w_1-plane with the cut or two-sided, semi-infinite barrier along OS_1BAS_2O.

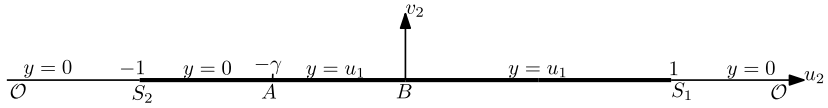

Fig. 3. The w_2-plane. The vortical region corresponds to the upper half-plane.

The solutions obtained below thus appear as "case 1" solutions of the 3-case taxonomy of Euler equation equilibria introduced in [19]. The presentation in these works show that $S(z)$ can be obtained by mapping the flow region to an auxiliary domain and considering the form of the mapping at special points on the boundary. In the present problem the form of the solution at all the special points is not immediately obvious and so the derivation below follows instead a hodograph mapping method [20].

Introduce the function

$$w_1(z) = v_1 + \mathrm{i}u_1 = (z - w_0(z))/2 = v + \mathrm{i}(y + u). \tag{10}$$

The usual complex velocity is $u_1 - \mathrm{i}v_1 = -\mathrm{i}w_1$ but, from (7), definition (10) gives the simple boundary condition on the unknown curve Γ,

$$u_1 = y, \qquad v_1 = 0 \qquad \text{on } \Gamma. \tag{11}$$

The flow is obtained by solving for z as a function of w_1 in the w_1, or hodograph, plane, sketched in Fig. 2. From (10), (11) the u_1 axis can be associated with y and the v_1 axis with x. The axes in Fig. 2 have been rotated anti-clockwise by $\pi/2$ to allow more economic labelling. Since w_1 is analytic in $\mathcal{D}$ (except at the origin) z is an analytic function of w_1 in the corresponding region of the w_1-plane except possibly at points corresponding to the origin or infinity. In particular, both x and y satisfy Laplace's equation in the hodograph plane and a complete problem can be set up for y as a function of u_1 and v_1.

Since $v_1 = 0$ on $y = 0$, (11) shows that the entire boundary of $\mathcal{D}$ lies along the line $v_1 = 0$ in the w_1-plane. Since the velocity is infinite at the origin in the z-plane, O maps to the point at infinity in the w_1-plane and the vortical flow region $\mathcal{D}$ maps to the entire w_1-plane. Fluid driven along the wall from the origin arrives at the stagnation point S_1 in $x < 0$ which, since the velocity vanishes there, corresponds to the origin in the w_1-plane. Since neighbouring fluid moves away from the wall ($v_1 > 0$) the segment OS_1 maps to the segment $u_1 < 0$, $v_1 = 0^+$ in the w_1-plane with $y = 0$ there. Fluid then passes around the boundary Γ of $\mathcal{D}$ to first reach the point of maximum width, denoted B here, where $y = 1$ by construction so $u_1 = 1$ by (11). Neighbouring fluid is again moving away from the wall ($v_1 > 0$) with $0 \le y \le b$ so the segment S_1B maps to the segment $v_1 = 0^+$, $0 \le u_1 \le 1$ in the w_1-plane with $y = u_1$ there, by (11). The boundary Γ then continues to the point at infinity in the z-plane, denoted A here, where the current has width $y = \alpha$ so $u_1 = \alpha$ by (11). Neighbouring fluid moves towards the wall ($v_1 < 0$) with $\alpha \le y \le 1$ so the segment BA maps to the segment $v_1 = 0^-$, $\alpha \le u_1 \le 1$ in the w_1-plane with again $y = u_1$ there. At A, y jumps to zero and remains there along the whole segment AO, passing through a second stagnation point at S_2. Neighbouring fluid moves towards the wall ($v_1 < 0$) so the segment AO maps to the segment $v_1 = 0^-$, $u_1 \le \alpha$ in the w_1-plane with $y = 0$ there.

Thus y satisfies Laplace's equation in the hodograph plane cut along the half-line $u_1 \le 1$, $v_1 = 0$, subject to

$$y = \begin{cases} 0 & (u_1 \le 0,\ v_1 = 0^+) \quad \text{and} \quad (u_1 \le \alpha,\ v_1 = 0^-) \\ u_1 & (0 < u_1 < 1,\ v_1 = 0^+) \quad \text{and} \quad (\alpha < u_1 < 1,\ v_1 = 0^-) \end{cases} \tag{12}$$

and a condition at infinity in w_1 that gives a dipole at O. Sufficiently close to O the velocity field is dominated by the dipole and so

$$z^2(u - \mathrm{i}v) \to -\mu/\pi + (Q/\pi\omega\ell^2)z + \mathcal{O}(z^2) \qquad \text{as } z \to 0, \tag{13}$$

where μ gives the dipole strength scaled on $2Q/\ell = \omega\ell$ and is real and positive for a dipole directed in the negative-x direction. The condition at infinity is thus, from (6) and (10),

$$z^2 w_1 \to -\mathrm{i}\mu/\pi \qquad \text{as } w_1 \to \infty. \tag{14}$$

The solution for y follows most simply by mapping the w_1-plane to the upper half of the w_2-plane through the mapping

$$w_2 = u_2 + \mathrm{i}v_2 = (1 + \mathrm{i}w_1)^{1/2}, \tag{15}$$

which maps the w_1-plane to the upper half of the w_2-plane (Fig. 3), opening the cut and converting the two-sided, semi-infinite barrier OB into the whole $v_2 = 0$ axis. The points at infinity, i.e. the origin O in the z-plane, correspond; the point B in the w_1-plane maps to the origin in the w_2-plane; the stagnation points $S_{1,2}$ split mapping to $u_2 = \pm 1$; and A, the point at infinity in the z-plane, maps to $u_2 = -\gamma$ where $\gamma = (1 - \alpha)^{1/2}$ is real and positive. The solution for z can then be written down by inspection (c.f. JM) as

$$z = (1/\pi)\{U(w_2)\log[(w_2 - 1)/(w_2 + \gamma)] + G(w_2)\} = F(w_2) \text{ (say)}, \tag{16}$$

where $U(w_2) = -\mathrm{i}w_1 = 1 - w_2^2$ and G is any function analytic in the upper half-plane whose imaginary part vanishes on $v_2 = 0$. In terms of w_2 the requirement (14) that there is a dipole at O becomes $z^2 w_2^2 \to \mu/\pi$ as $w_2 \to \infty$. The first term in parentheses in (16) has the expansion,

$$(1+\gamma)w_2 + (1-\gamma^2)/2 - (2-\gamma)(1+\gamma)^2/(3w_2) + O(w_2^{-2}), \qquad w_2 \to \infty. \tag{17}$$

Thus $G(w_2) = -(1 + \gamma)w_2 - (1 - \gamma^2)/2$ and $\mu = (1/9\pi)(2 - \gamma)^2(1 + \gamma)^4$, completing the solution for the flow.

Fig. 4 shows the relative current width α as a function of the scaled dipole strength μ. As $\alpha \to 0^+$, i.e. $\gamma \to 1^-$, this solution reduces to that for a pure dipole, given in JM, with here $\mu = 16/9\pi \approx 0.5659$. As α increases, i.e. γ decreases, the position where the current is broadest moves monotonically from $x = 0$ when $\alpha = 0$ to $x = \infty$ when $\alpha = 1$, $\gamma = 0$

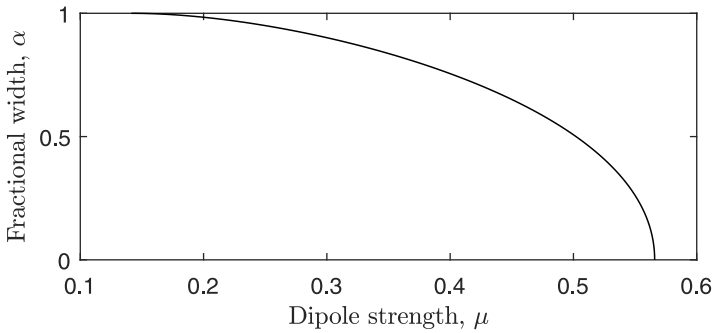

Fig. 4. The width of the downstream current as a fraction, α, of the width of the bulge as a function of the dipole strength, μ, scaled on the expelled vorticity, with $4/9\pi < \mu \le 16/9\pi$ for bulging outflows.

and $\mu = 4/9\pi \approx 0.1415$. The strength of the dipole decreases monotonically and the region of recirculating flow near the origin, driven by the dipole, shrinks. Appendix A shows that for weaker dipoles, $\mu \le 4/9\pi$, the geometry in the hodograph plane is modified to give a solution that smoothly joins that of (16) with $\gamma = 0$ to that of the pure source in JM when $\mu = 0$.

Since $v_1, v_2 = 0$ on Γ, $w_2 = u_2 = \pm(1-u_1)^{1/2} = \pm(1-y)^{1/2}$ there, giving the explicit expression for Γ,

$$x = (1/\pi)\{y \log\left[\frac{1 \mp (1-y)^{1/2}}{\gamma \pm (1-y)^{1/2}}\right] \mp (1+\gamma)(1-y)^{1/2} - (1-\gamma^2)/2\}, \tag{18}$$

with upper/lower signs associated.

Fig. 5 shows outflow current boundaries for different values of the relative dipole strength μ. Except for Fig. 7, this and subsequent plots are isotropic with the same x and y plotting scales. Here, and in subsequent figures, the length scale has been taken to be the downstream current width, $(2Q/\omega)^{1/2}$, so the coordinates are $(x^*, y^*)(\omega/2Q)^{1/2} = (x, y)/\alpha$, equivalent to taking $\ell = (2Q/\omega\alpha^2)^{1/2}$. With this scaling, in accord with Fig. 4, as μ increases from $\mu = 4/9\pi$ the outflow bulge becomes larger relative to the current width, becoming infinite when $\mu = 16/9\pi$, when the dimensional current width vanishes and the dimensional dipole strength $\mu* = \omega/\alpha^3$ becomes infinite for nonzero ω.

Near the front stagnation point, $y \ll 1$ and (18) gives

$$x = \frac{\pi}{8}(\gamma^2 - 2\gamma - 3) + \frac{\pi y}{8}\left[1 + \gamma + 2\log\left(\frac{y}{2+2\gamma}\right)\right] + O(y^2), \tag{19a}$$

$$\frac{\mathrm{d}x}{\mathrm{d}y} = \frac{\pi}{8}(3+\gamma) + \frac{\pi}{4}\log\left(\frac{y}{2+2\gamma}\right) + O(y). \tag{19b}$$

The front stagnation point thus lies at $x = \pi(\gamma^2 - 2\gamma - 3)/8$ and, as $\mathrm{d}x/\mathrm{d}y$ diverges logarithmically to negative infinity as $y \to 0^+$, the interior angle between the boundary Γ and the positive-x direction is $\theta_s = \pi$: Γ forms a cusp with its image in the wall. In the closely related problem of a vortex patch propagating steadily along a wall, Saffman and Tanveer [21] and Overman [22] show that the patch boundary meets the wall perpendicularly (corresponding to $\theta_s = \pi/2$ here). The difference arises from the presence of a non-zero external flow in the co-moving frame of the propagating patch which determines the form of the solution local to the leading stagnation point. The absence of external flow in the outflow problem changes the local form to that in (19). Here, and for the propagating patch, the boundary curvature is infinite at the wall.

Streamlines for the flow can be obtained straightforwardly by following JM and differentiating (16) to give the particle path

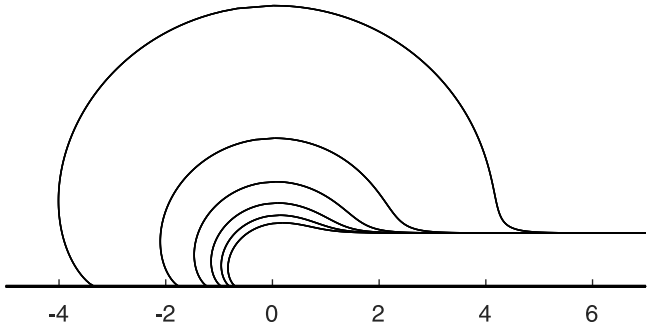

Fig. 5. Outflow current boundaries for different relative dipole strengths μ. Horizontal distances are scaled on the downstream current width, $(2Q/\omega)^{1/2}$, and plotted isotropically here and below. The bulge width increases with increasing μ with here $\gamma = 0.4$, 0.5, 0.6, 0.7, 0.8 and 0.9 and $\mu = 0.35$, 0.40, 0.45, 0.50, 0.53 and 0.56.

equation

$$\dot{z} = F'(w_2)\dot{w}_2, \tag{20}$$

where

$$\dot{z} = u + \mathrm{i}v = \mathrm{i}\overline{w}_1 - y = \overline{w}_2^2 - 1 - \Im\{F(w_2)\} = w \text{ (say)}, \tag{21}$$

from (6), (10) and (15), with overbar denoting complex conjugate and $\Im$ imaginary part. Rearranging (20) and (21) gives the first order scalar ordinary differential equation

$$\dot{w}_2 = w/F'(w_2). \tag{22}$$

As the right side is known explicitly, (22) can be integrated simply numerically to give the particle paths in the w_2-plane with the corresponding streamlines in the z-plane given by $z = F(w_2)$. Since speeds become arbitrarily large near the source it is useful for practical integrations to change the independent variable in the integrations to the arc length s (say) along the streamline in the original domain, so $\mathrm{d}s = |u + \mathrm{i}v|\mathrm{d}t$ and

$$\frac{\mathrm{d}w_2}{\mathrm{d}s} = w/[|w|F'(w_2)]. \tag{23}$$

Fig. 6 gives streamlines computed using (23) for the largest value in Fig. 6, $\gamma = 0.9$ for which $\mu = 0.5577$ and $\alpha = 0.19$, giving a bulge width scaled on the current width of 5.26. Near the origin the flow is dominated by the irrotational dipole directed in the negative-x direction and only away from this region, over non-dimensional distances of order unity corresponding to dimensional distances of order the vortical length scale $(2Q/\omega)^{1/2}$, does the fluid vorticity become important. The dipole sets up a closed region of anticyclonic recirculating fluid, a feature that has been noted in both experiments [9] and simulations [10].

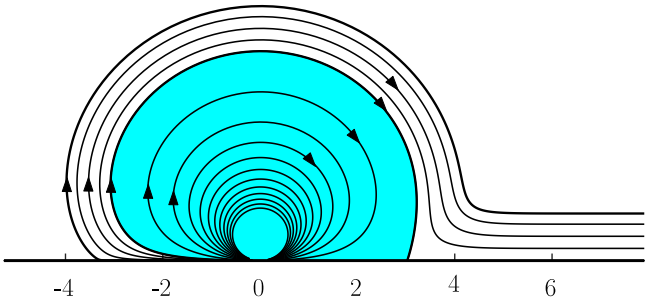

Fig. 6. The exact steady state for a source of positive vorticity fluid at the origin with a superposed irrotational opposing dipole. The outer zero streamline, marking the boundary of the expelled fluid, is thickened as is the streamline separating the blue-shaded anticyclonic recirculating fluid from the escaping fluid. Here $\gamma = 0.9$.

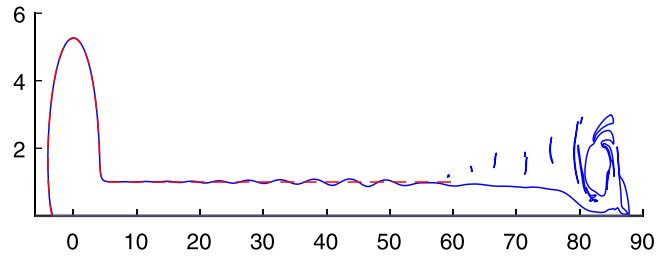

Fig. 7. The outflow boundary (solid blue line) at time $t = 240$ for the initial value problem of a dipole with $\gamma = 0.9$. The length scale has been chosen to give a coastal current of unit width. The dashed (red) line gives the outflow boundary for the corresponding steady solution of Fig. 6. The vertical scale of the plot has been exaggerated by a factor of 16.

4. Perturbations of the steady state

The robustness of the exact steady solution (Section 3) can be assessed by considering the effects of small perturbations to the flow. JM note that in the linear approximation this corresponds to introducing a vortex sheet along Γ and gives precisely the problem of topographic wave evolution along an escarpment of height unity lying along Γ [23,24]. Downstream, i.e. for $x \gg 1$, Γ can be taken as the straight line $y =$constant, giving a real-valued dispersion relation for all wavelengths. All disturbances are neutrally stable, propagating to the right with longer waves travelling faster.

Sufficiently close to the stagnation point S_1 the presence of the wall affects the form of the waves and the geometry becomes one of an escarpment abutting a wall, considered previously for a straight escarpment perpendicular to a wall [23] and a semi-circular escarpment [25]. The waves move away from the stagnation point, speeding up, lengthening and decreasing in energy density as they do so.

For a pure dipole in the absence of a source flow the current boundary reattaches to the wall at a downstream stagnation point (the reflection about the origin of the upstream stagnation point). The solutions in [23,25] show that small disturbances propagate towards this reattachment point magnifying in energy density (although not amplitude, in the linear approximation) as they slow approaching it. JM investigated whether these perturbations could disrupt the steady solution at the rear stagnation point, noting that the steady dipole solution appears stable over long times to sufficiently small but finite perturbations. For larger perturbations the dipoles were all eventually disrupted with the time until the disruption was significant increasing without limit as the size of the perturbation amplitude decreased. JM concluded that the steady dipole solution is unstable at sufficiently large times due to finite amplitude perturbations accumulating at the wall at the rear stagnation point.

The absence of a reattachment point when any source flow is present suggests that steady flow in the presence of a source is stable with perturbations taking the form of neutral waves of bounded energy density. The numerical integrations of the initial value problem in Section 5 bear this out.

5. The initial value problem

The initial value problem for the full unsteady system of Section 2 can be integrated numerically to high accuracy using the method of contour dynamics [26–28] by parametrising only the boundary Γ of the outflow. The code used here, described in detail in [29], allows integrations to be continued to large times with practically no loss of accuracy by allowing boundary contours to break and join through contour surgery. As in JM, the solid wall is incorporated by introducing an equal and opposite vortex patch in $y < 0$ and then using the unbounded domain method with these two patches. The source and dipole are incorporated by adding the velocity components for an irrotational dipole and an irrotational isotropic source to the velocity components computed from the vortex patches. The expelled fluid is taken to have unit vorticity ($\omega = 1$), determining the timescale through (1), with higher vorticity simply giving faster propagation. The volume flux is taken as $Q = 0.5$ to give a downstream current of width unity. Increasing Q increases the current width. The dipole strength is taken to correspond to the value $\gamma = 0.9$ of Fig. 6, giving $\alpha = 0.19$, $\mu = 0.5577$ and thus a dimensional dipole strength $\mu^* = \mu\omega\ell^3 = \mu\omega/\alpha^3 = 81.31$. The vortex is started as a semi-circle of radius 0.1, as in Fig. 1(a), to avoid the singular velocities at the origin associated with the source and dipole. The results are independent of the radius of the initial semi-circle provided it is sufficiently small but larger than the discretisation length of the boundary curve Γ. The source is switched on impulsively at $t = 0$ but, to avoid the large velocities associated with the dipole drawing the current's downstream boundary into the origin, the dipole strength is ramped up using

$$\hat{\mu}(t) = \mu^* \sin(\pi t/2T), \quad 0 \le t \le T; \qquad \hat{\mu}(t) = \mu^*, \quad t > T, \tag{24}$$

with $T = 200$. The boundary is advected using a 4th-order Runge–Kutta method with a timestep of 0.1 (with smaller timesteps producing graphically indistinguishable results). At each Runge–Kutta substep it is sufficient to compute the position of only the patch in $y \ge 0$ as the position of the patch in $y < 0$ follows by symmetry (although the boundary integral for the velocity must be evaluated along both patch boundaries). Points are redistributed along the contour after each timestep based on the curvature of the contour with the leading and trailing points initially on the wall constrained to remain on the wall. Contour surgery acts only on patches with the same value of vorticity and so there is no interaction between the patches in $y \ge 0$ and $y < 0$. The entire material curve surrounding the expelled fluid is discretised and followed throughout the whole evolution. The infinite space Laplacian Green's function is used in the boundary integral and so no additional boundary conditions are required on the open boundaries.

Initially the flow develops similarly to the pure source evolution of JM: the region of expelled fluid grows to form an elongated eddy whose head splits off and propagates away to the right under the influence of its image in the wall, the current established behind the leading eddy rapidly settles down to oscillate about the exact steady solution with the oscillations taking the form of

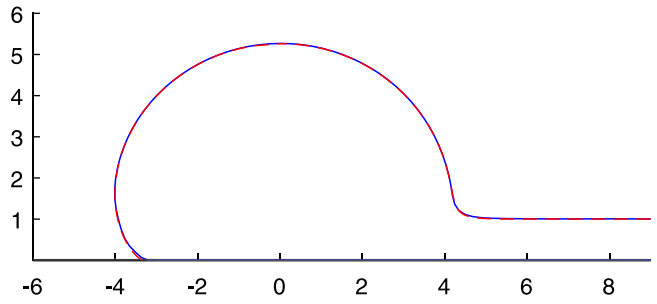

Fig. 8. The portion of Fig. 7 in the neighbourhood of the origin plotted isotropically, without vertical exaggeration.

long waves of diminishing amplitude and increasing wavelength propagating to the right along the interface between vortical and irrotational fluid, as expected from the discussion of Section 4. As the dipole strengthens the bulge near the origin grows towards the corresponding steady solution and at $t = T$ the curves are graphically indistinguishable for $x < 10$. Fig. 7 shows the outflow boundary at $t = 240$. The eddy formed at the impulsive starting of the source lies between $x = 80$ and $x = 90$ with small regions of shed vorticity visible in $x > 60$. The neutral waves propagating along the outflow boundary are long, with wavelengths of order 8 current widths. Fig. 8 gives the portion of Fig. 7 near the origin, showing that in this region the initial value problem has converged to the steady solution. In fact there is no graphically discernible change in the outflow boundary for $t > T$.

6. Discussion

Section 3 and Appendix A extend the solution for a source of vortical fluid against a wall given in JM to include the effect of an irrotational dipole superposed on the source and directed in the opposite direction to the ensuing vortical coastal current. For sufficiently strong dipoles this leads to a bulging outflow containing a closed anticyclonic recirculating region of similar form to those observed in experiments and numerical simulations of the full equations. Numerical integration of the governing unsteady Euler equations using contour dynamics shows that the steady solution is the final state of an initial value problem, verifying the numerics, scalings and analysis and, incidentally, showing that the final steady state is numerically stable. The flow rapidly becomes steady within any finite region of the origin over times sufficient for initial transients to be advected downstream.

The dipole imparts no net downstream momentum to the fluid and so the argument of Johnson et al. [5] and Southwick et al. [14] applies directly showing that the downstream momentum imparted to the flow by the source precisely matches that carried away by the coastal current and the argument supporting expanding outflows in [13] does not apply. Equally, knowledge of a small number of bulk quantities, such as the mass and momentum fluxes, is not sufficient to determine the shape of the flow near the outflow and more detailed knowledge of the outflow velocity profile is needed [30].

Declaration of competing interest

The authors declare that they have no known competing financial interests or personal relationships that could have appeared to influence the work reported in this paper.

Data availability

No data was used for the research described in the article.

Acknowledgements

The author would like to thank the Isaac Newton Institute for Mathematical Sciences, Cambridge, for support and hospitality during the programme "Complex analysis: techniques, applications and computations" where work on this paper was undertaken. This work was supported by EPSRC, United Kingdom grant EP/R014604/1 and the UK Natural Environment Research Council under grant number NE/S009922/1. The author is indebted to Professor Dritschel for providing a copy of his code that formed the basis for the code developed here and to Professor Crowdy for suggestions that improved the exposition.

Appendix A. Weak dipoles, $\mu \le 4/9\pi$

Section 3 shows that as α increases from 0 to 1 and the dipole weakens from $\mu = 16/9\pi$, where the coastal current disappears, to $\mu = 4/9\pi$, the position where the current is broadest moves monotonically from $x = 0$ to $x = \infty$. Simultaneously, the co-located position of maximum downstream flow on the vortex boundary moves from $x = 0$ to $x = \infty$. For weaker dipoles this boundary speed maximum, where $u = c^2$ (say) for $c > 1$, larger than the unit value at $x = \infty$, occurs on $y = 0$ at some point C which moves back from $x = \infty$ when $\mu = 16/9\pi$ to reach the origin when $\mu = 0$. Fig. A.9 gives the w_1 hodograph plane for this flow. The cut along $v_1 = 0$ now extends to $u_1 < c^2$ and A lies at $u_1 = 1$. The entire curved boundary Γ, on which $y = u_1$, maps to the segment S_1A, with the remainder of the cut corresponding to the vortex boundary $y = 0$. Along CO fluid moves towards the wall dominated by the dipole flow, so $v_1 = 0^-$ but along AC fluid moves away from the wall dominated by the expanding source flow, so $v_1 = 0^+$. The boundary conditions on y on the cut are thus

$$y = \begin{cases} 0 & (u_1 \le 0 \text{ and } 1 < u_1 \le c^2,\ v_1 = 0^+) \quad \text{and} \quad (u_1 \le c^2,\ v_1 = 0^-) \\ u_1 & (0 \le u_1 < 1,\ v_1 = 0^+). \end{cases} \tag{A.1}$$

The required mapping to the upper half of the w_2-plane is then

$$w_2 = (c^2 + \mathrm{i}w_1)^{1/2}. \tag{A.2}$$

Again the points at infinity correspond; the point C maps to the origin; the stagnation points split mapping to $u_2 = \pm c$; and A maps to $u_2 = \gamma_w = (c^2-1)^{1/2}$ which is real and positive, sketched in Fig. A.10. Similarly to Section 3 this gives

$$z = (1/\pi)\{U_w(w_2)\log[(w_2 - c)/(w_2 - \gamma_w)] + G_w(w_2)\} = F_w(w_2) \text{ (say)}, \tag{A.3}$$

where $U_w(w_2) = -\mathrm{i}w_1 = c^2 - w_2^2$ and G_w is any function analytic in the upper half-plane whose imaginary part vanishes on $v_2 = 0$. The first term in parentheses in (A.3) has the expansion,

$$(c - \gamma_w)w_2 + 1/2 + [(2c^2+1)\gamma_w - 2c^3]/(3w_2) + O(w_2^{-2}), \qquad w_2 \to \infty. \tag{A.4}$$

Thus $G(w_2) = (\gamma_w - c)w_2 - 1/2$ and $\mu = (1/9\pi)[(2c^2+1)\gamma_w - 2c^3]^2$, completing the solution for the flow. For $c = 1$, $\gamma_w = 0$ and (A.3) gives (16) with $\gamma = 0$, i.e. $\alpha = 1$, as required.

Since $w_2 = u_2 = (c^2 - y)^{1/2}$ on Γ, (A.3) gives the explicit equation for the vortex boundary

$$\pi x = y\log[(c - (c^2-y)^{1/2})/((c^2-y)^{1/2} - \gamma_w)] + (\gamma_w - c)(c^2-y)^{1/2} - 1/2, \tag{A.5}$$

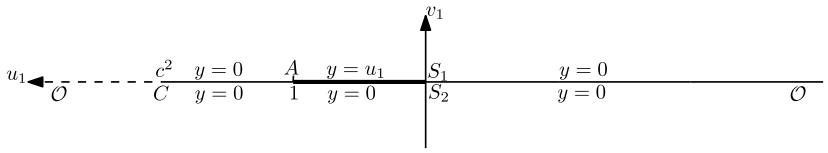

Fig. A.9. The cut hodograph w_1-plane for the weak dipole with the cut along OS_1ACS_2O.

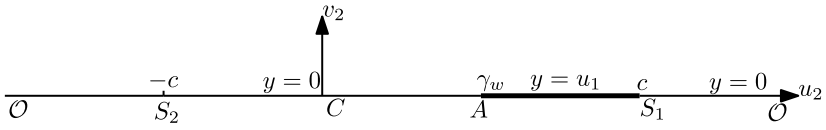

Fig. A.10. The w_2-plane for the weak dipole. The vortical region corresponds to the upper half-plane.

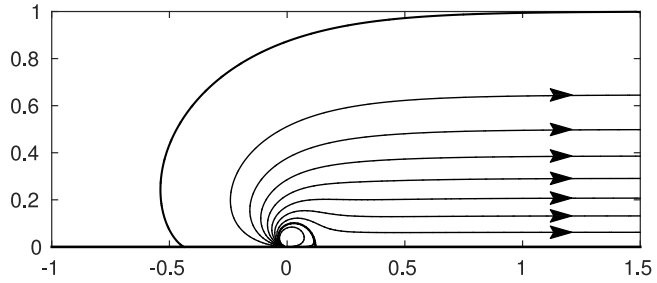

Fig. A.11. The exact steady state for a source of positive vorticity fluid at the origin with superposed opposing dipole. Evenly spaced streamlines are shown with the outer zero streamline, marking the boundary of the expelled fluid, and the streamline separating recirculating and escaping fluid, shown thickened as in Fig. 6. Here $c = 1.01$ in (A.3) and the recirculating region is already weak.

$0 \le y < 1$. For $c = 1$, (A.5) reduces to solution (18) with $\gamma = 0$ as required; and for $c \to \infty$ (A.5) reduces to

$$x = -[1 + y\log(1/y - 1)]/\pi, \qquad 0 \le y < 1, \tag{A.6}$$

the solution for a pure source in JM. Fig. A.11 gives streamlines for the flow when $c = 1.01$. Even for this almost minimum value for solution (A.3) the recirculating region is negligible, vanishing as $c \to \infty$.

Appendix B. An unequal source–sink pair

The same general flow pattern as above for a source at the origin with a superposed opposing dipole can be obtained by considering a source at the origin with a weaker sink located on the wall downstream from the source. Thus let there be a source of strength $Q(1+\delta)$ at the origin, $\mathcal{O}$, and a sink of strength $Q\delta$ at $\mathcal{O}_2$, for $x = \sigma > 0$, where ℓ is again the maximum width of the current, horizontal lengths are scaled on ℓ, the expelled fluid has vorticity ω and the downstream current has width α as in Section 2. In the neighbourhood of $\mathcal{O}$ and $\mathcal{O}_2$ the velocity field has the form (c.f (13))

$$z(u - \mathrm{i}v) \to Q(1+\delta)/\pi\omega\ell^2 + \mathcal{O}(z) \quad \text{as } z \to 0, \tag{B.1a}$$

$$(z - \sigma)(u - \mathrm{i}v) \to -Q\delta/\pi\omega\ell^2 + \mathcal{O}(z - \sigma) \quad \text{as } z \to \sigma. \tag{B.1b}$$

The velocity along the wall is infinite at $\mathcal{O}$ and $\mathcal{O}_2$ falling to a minimum greater than 1 at a point between $\mathcal{O}$ and $\mathcal{O}_2$. Denote this point by B_2 and the speed there by β. Fig. B.12 gives the w_1 hodograph plane for this flow. The boundary conditions on y along $OS_1BAS_2O_2$ are precisely those in Fig. 2 along OS_1BAS_2O. The additional cut along OB_2O_2 simply gives the speed decreasing from its infinite value at the source $\mathcal{O}$ to its local minimum of β at B_2 before increasing back to infinity at $\mathcal{O}_2$. Writing

$$\hat{w}_1 = 2(w_1 - \mathrm{i})/(\beta - 1) - \mathrm{i}, \qquad w_1 = (\beta - 1)(\hat{w}_1 + \mathrm{i})/2 + \mathrm{i}, \tag{B.2}$$

translates the gap in Fig. B.12 along the v_1 axis and dilates it so that the gap fills the segment $|u_1| < 1$. Then the Joukowski mapping

$$w_2 = \mathrm{i}[\hat{w}_1 \pm (\hat{w}_1^2 + 1)^{1/2}], \qquad \hat{w}_1 = -\mathrm{i}(w_2 + 1/w_2)/2, \tag{B.3}$$

opens both cuts, mapping the cut $\hat{w}_1$ plane to the upper half of the w_2 plane (Fig. B.13), with the minus sign corresponding to the half plane $v_1 < 0$ and the plus sign corresponding to $v_1 > 0$. The points A, S_1 thus map to $w_2 = a, s_1$ where $a = \hat{a} - (\hat{a}^2 - 1)^{1/2}$, $s_1 = \hat{s} + (\hat{s}^2 - 1)^{1/2}$ for $\hat{a} = 1 - 2(\alpha - 1)/(\beta - 1)$ and $\hat{s} = (\beta + 1)/(\beta - 1)$. This gives the solution for z as

$$z = (1/\pi)\{U_s(w_2)\log[(w_2 - s_1)/(w_2 - a)] + G_s(w_2)\} = F_s(w_2) \text{ (say)}, \tag{B.4}$$

where $U_s(w_2) = -\mathrm{i}w_1 = (\beta+1)/2 - (\beta-1)(w_2 + 1/w_2)/4$ and G_s is any function analytic in the upper half-plane whose imaginary part vanishes on $v_2 = 0$. Expanding the first term in parentheses in (B.4) near $\mathcal{O}_2$ and $\mathcal{O}$ gives

$$U_s(w_2)\log\left(\frac{w_2 - s_1}{w_2 - a}\right) = \begin{cases} C_1/w_2 + C_2 + C_3 w_2 + O(w_2^2), & w_2 \to 0, \\ C_4 + C_5/w_2 + O(w_2^{-2}), & w_2 \to \infty, \end{cases} \tag{B.5}$$

where

$$\begin{aligned} C_1 &= [(1-\beta)/4]\log(s_1/a), \\ C_2 &= (\beta-1)(a-s_1)/4as_1 + [(1+\beta)/2]\log(s_1/a), \\ C_3 &= (a-s_1)[(\beta-1)(a+s_1) - 4as_1(1+\beta)]/8a^2s_1^2 \\ &\quad -[(\beta-1)/4]\log(s_1/a), \\ C_4 &= (\beta-1)(s_1-a)/4, \\ C_5 &= (a-s_1)[4(\beta+1) - (\beta-1)(a+s_1)]/8. \end{aligned} \tag{B.6}$$

In terms of w_2, the asymptotic forms (B.1) give

$$z = \begin{cases} -[4Q(1+\delta)/\pi(\beta-1)\omega\ell^2]/w_2 + O(w_2^2), & w_2 \to 0 \\ -[4Q(1+\delta)/\pi(\beta-1)\omega\ell^2]/w_2 + O(w_2^{-2}), & w_2 \to \infty. \end{cases} \tag{B.7}$$

Comparing (B.5) and (B.7) gives $G_s(w_2) = -C_4 - C_1/w_2$, $\sigma = (C_2 - C_4)/\pi$, $Q(1+\delta)/\omega\ell^2 = -(\beta-1)C_5/4$ and $Q\delta/\omega\ell^2 = (\beta-1)C_3/4$. This completes the solution in terms of the fractional current width α and the speed β. More natural variables are perhaps α and the source–sink displacement σ which can be obtained by numerically inverting the equation for σ.

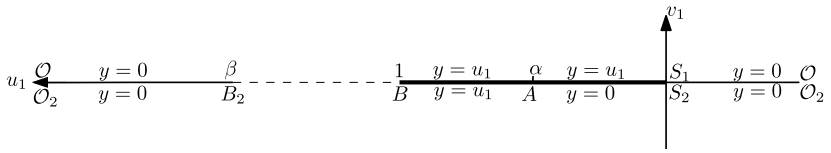

Fig. B.12. The cut hodograph w_1-plane for the source–sink pair with a cut along $OS_1BAS_2O_2$ as in Fig. 2 and a second cut along OB_2O_2.

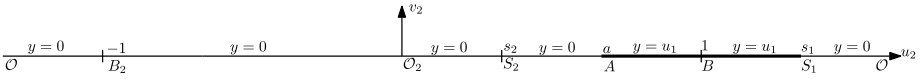

Fig. B.13. The w_2-plane for the source–sink pair. The vortical region corresponds to the upper half-plane.

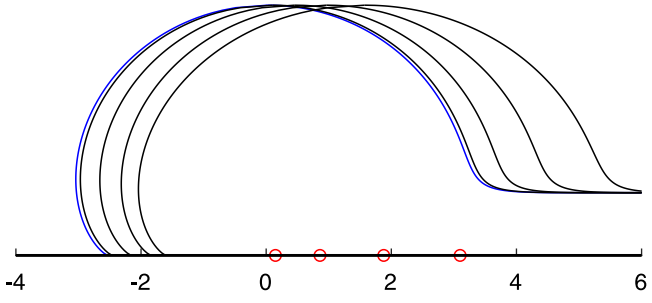

β	σ	Q	δ	$\sigma\delta$	$\hat{\sigma}$
2	0.775	1.047	0.808	0.6260	3.100
4	0.470	2.419	1.228	0.5768	1.879
16	0.215	16.034	2.581	0.5550	0.860
512	0.037	2708.5	14.869	0.5511	0.148

Fig. B.14. Profiles of the current edge in source–sink flow. The source is at the origin and the red circles give the locations for the sink. With increasing β the sink moves towards the origin and the product $\sigma\delta$ approaches the corresponding dipole strength $\mu = 0.5514$ (with profile shown in blue).

On Γ, $v_2 = 0$ so $w_2 = u_2 = [1 + \beta - 2y \pm 2((\beta - y)(1 - y))^{1/2}]/(\beta - 1)$ and (B.4) gives the explicit equation for the vortex boundary

$$x = (1/\pi)\{y \log[(u_2 - s_1)/(u_2 - a)] - C_4 - C_5/u_2\}, \qquad 0 \le y < 1. \tag{B.8}$$

Fig. B.14 gives profiles of the current edge and corresponding derived flow quantities for various values of β.

References

[1] I. Lake, K. Borenäs, P. Lundberg, Potential-vorticity characteristics of the Faroe Bank Channel deep-water overflow, J. Phys. Oceanogr. 35 (2005) 921–932.

[2] R. Beardsley, R. Limeburner, H. Yu, G. Cannon, Discharge of the changjiang (yangtze river) into the east China sea, Cont. Shelf Res. 4 (1985) 57–76.

[3] M.A. Spall, J.F. Price, Mesoscale variability in Denmark Strait: the PV outflow hypothesis, J. Phys. Oceanogr. 28 (1998) 1598–1623.

[4] G.M. Marques, L. Padman, S.R. Springer, S.L. Howard, T.M. Özgökmen, Topographic vorticity waves forced by Antarctic dense shelf water outflows, Geophys. Res. Lett. 41 (2014) 1247–1254.

[5] E.R. Johnson, O.R. Southwick, N.R. McDonald, The long-wave vorticity dynamics of rotating buoyant outflows, J. Fluid Mech. 822 (2017) 418–443.

[6] S. Jamshidi, E.R. Johnson, Coastal outflow currents into a buoyant layer of arbitrary depth, J. Fluid Mech. 858 (2019) 656–688.

[7] R. Hide, On source-sink flows in a rotating fluid, J. Fluid Mech. 32 (1968) 737–764.

[8] E.R. Johnson, N.R. McDonald, Vortical source-sink flow against a wall: The initial value problem and exact steady states, Phys. Fluids 18 (2006) 076601.

[9] P.J. Thomas, P.F. Linden, Rotating gravity currents: small-scale and large-scale laboratory experiments and a geostrophic model, J. Fluid Mech. 578 (2007) 35–65.

[10] S. Gregorio, D. Haidvogel, P. Thomas, E. Taskinoglu, A. Skeen, Laboratory and numerical simulations of gravity-driven coastal currents: Departures from geostrophic theory, Dyn. Atmos. Oceans 52 (1) (2011) 20–50.

[11] J.P. McCreary, S.L. Zhang, S.R. Shetye, Coastal circulations driven by river outflow in a variable density 1 1/2-layer model, J. Geophys. Res. -Oceans 102 (1997) 15535–15554.

[12] Z. Liu, J. Gan, Z. Cai, Ballooning of surface-advected freshwater bulge in a rotating frame, J. Geophys. Res. Oceans 128 (2023).

[13] D. Nof, T. Pichevin, The ballooning of outflows, J. Phys. Oceanogr. 31 (2001) 3045–3058.

[14] O.R. Southwick, E.R. Johnson, N.R. McDonald, Potential vorticity dynamics of coastal outflows, J. Phys. Oceanogr. 47 (2017) 1021–1041.

[15] L.M. Milne-Thomson, Theoretical Hydrodynamics, Macmillan, New York, 1955.

[16] S.D. Howison, J.R. King, Explicit solutions to six free-boundary problems in fluid flow and diffusion, IMA J. Appl. Math. 42 (1989) 155–175.

[17] D. Crowdy, A class of exact multipolar vortices, Phys. Fluids 11 (1999) 2556–2564.

[18] D.G. Crowdy, Solving Problems in Multiply Connected Domains, in: NSF-CBMS Conference Series in Applied Mathematics, SIAM, 2020.

[19] D.G. Crowdy, Exact solutions for steadily travelling water waves with submerged point vortices, J. Fluid Mech. 954 (2023) A47.

[20] S.D. Howison, Complex variables in industrial mathematics, in: H. Neunzert (Ed.), Proceedings of the Second European Symposium on Mathematics in Industry, Oberwolfach, Teubner, Stuttgart, 1987.

[21] P.G. Saffman, S. Tanveer, The touching pair of equal and opposite uniform vortices, Phys. Fluids 25 (1982) 1929–1930.

[22] E. Overman, Steady-state solutions of the Euler equations in two dimensions II. local analysis of limiting V-States, SIAM J. Appl. Math. 46 (1986) 765–800.

[23] E.R. Johnson, Topographic waves and the evolution of coastal currents, J. Fluid Mech. 160 (1985) 499–509.

[24] K.L. Swanson, P.J. Kushner, I.M. Held, Dynamics of barotropic storm tracks, J. Atmos. Sci. 54 (1997) 791–810.

[25] R.G.A. Hurst, E.R. Johnson, Rapid formation of Taylor-columns - obstacles against sidewalls, Geophys. Astrophys. Fluid Dyn. 52 (1990) 105–124.

[26] G.S. Deem, N.J. Zabusky, Vortex waves: stationary 'V-states', interactions, recurrence, and breaking, Phys. Rev. Lett. 40 (1978) 859–862.

[27] N.J. Zabusky, M. Hughes, K. Roberts, Contour dynamics for the Euler equations in two dimensions, J. Comput. Phys. 30 (1979) 96–106.

[28] P.G. Saffman, Vortex Dynamics, CUP, 1992.

[29] D.G. Dritschel, Contour surgery: A topological reconnection scheme for extended integrations using contour dynamics, J. Comput. Phys. 77 (1) (1988) 240–266.

[30] S. Jamshidi, E.R. Johnson, Vortex competition in coastal outflows, J. Mar. Res. 77 (3–4) (2019) 325–349.